75th International Astronautical Congress (IAC), Milan, Italy, 14-18 October 2024.


IAC-24-A2.IP.14

# In-Space Manufacturing of Functional Sensors

**Justin Astacio[a], M. Laura Sorgi Johann[b], Zachary Stein[c], Leonardo Facchini[d], Janine Wischek[e], Marion Bartsch[f], Michael Kinzel[g], Seetha Raghavan[h*]**

[a] *Department of Aerospace Engineering, Embry-Riddle Aeronautical University, Daytona Beach, Florida, United States*, ASTACIJ1@my.erau.edu
[b] *Department of Aerospace Engineering, Embry-Riddle Aeronautical University, Daytona Beach, Florida, United States*, SORGIJOM@my.erau.edu
[c] *Department of Aerospace Engineering, Embry-Riddle Aeronautical University, Daytona Beach, Florida, United States*, STEINZ@my.erau.edu
[d] *Institute of Materials Physics in Space, German Aerospace Center (DLR), Linder Höhe*, *Cologne, Germany* Leonardo.Facchini@dlr.de
[e] *Institute of Materials Research, German Aerospace Center (DLR), Linder Höhe*, *Cologne, Germany* janine.wischek@dlr.de
[f] *Institute of Materials Research, German Aerospace Center (DLR), Linder Höhe*, *Cologne, Germany* Marion.Bartsch@dlr.de
[g] *Department of Aerospace Engineering, Embry-Riddle Aeronautical University, Daytona Beach, Florida, United States*, KINZELM@erau.edu
[h] *Department of Aerospace Engineering, Embry-Riddle Aeronautical University, Daytona Beach, Florida, United States*, seetha.raghavan@erau.edu
* Corresponding Author

**Abstract**

Human exploration beyond Earth's atmosphere is rapidly increasing and with it the need for supporting research and technology in the field. Among these, in-space manufacturing of functional materials, specifically those that possess sensing properties, is a significant but valuable challenge. This work explores two different manufacturing processes applied to lunar mare simulant (LMS-1D), towards the creation of functional sensors where optical emissions via spectroscopy have the potential to offer temperature or stress/damage sensing capabilities. Resin-based 3D printing using Digital Light Processing (DLP) was used to produce 10% wt fraction of regolith composite samples. A second approach of manufacturing binderless green parts and sintering at 1150°C was used to produce consolidated pure regolith sintered samples. Raman spectroscopy results, compared with raw powder, show that some distinct mineral peaks for both consolidated DLP samples and sintered samples were conserved. Intrinsic spectral emission intensities were seen to vary with the manufacturing process with lower or loss of intensities observed in pure regolith sintered samples, attributed to sintering. Compressive test results for the pure regolith sintered samples showed a scatter in compressive strength with an average of 67.4 MPa and a standard deviation of 25.3 MPa. The initial findings demonstrate the viability of sensor development using these manufacturing approaches. The findings demonstrate also the potential for selectively manufacturing regolith materials with compositions that exhibit the desired sensitivity for tailored sensor functionality. The outcomes will offer a pathway to manufacture new functional materials from in-situ resources to meet space and earth-based needs.

**Keywords:** In-space manufacturing, Regolith Manufacturing, Raman Spectroscopy, In-situ Resource Utilization

**Acronyms/Abbreviations**

LMS – Lunar Mare Simulant
LHS – Lunar Highland Simulant
DLP – Digital Light Processing

## 1. Introduction

Goals for sustained extra-terrestrial human presence have greatly accelerated research and development of materials and structures that support life beyond earth. This includes the use of in-situ resources, such as lunar and planetary regolith, to develop structural materials for habitats, landing pads, and other infrastructure in low gravity environments. Materials for construction have been developed by converting regolith into geopolymers with alkaline solutions like sodium silicate [1]. The compressive strength of lunar regolith geopolymers can reach 18–30 MPa, making them suitable for in-situ construction on the Moon [1]. Recent work explored the effect of sintering temperature in the manufacturing of

lunar and Martian regolith demonstrating the optimal sintering temperature is somewhere between 1100 °C and 1200 °C [2]. In addition to construction materials, regolith is also being investigated for producing oxygen and metals. Lunar regolith has high oxide content which can be extracted to provide oxygen for life support and fuel [3]. In addition, metals including aluminium and iron can be produced as by-products while processing regolith, and these can be used for building components in space [3].

Significant focus has, therefore, been on designing structural materials with lunar and planetary regolith. However, safe long-duration exploration will require the creation of functional materials from in-situ resources. It is important to investigate the properties of these extraterrestrial materials that can be leveraged in support of the various systems needed to maintain a human presence on the Moon. Of key interest are the design of sensors, tailored to identify damage in supporting structures or monitor significant temperature or pressure changes [5]. The use of in-situ resources to create such sensors in space is the motivation of this effort.

*1.1 Lunar regolith properties*

LMS-1D is a simulant of regolith from the Mare regions of the lunar surface which is known for its basalt-rich composition. The "D" or dust variant represents fine dust which is created when surface regolith is pulverized by meteor impacts over a significant period of time [2]. The uncompressed density of LMS-1D is 0.7 g/cm$^3$, mean particle size is 7 μm with the particle size range up to 32 μm. The morphology of the simulant is representative of the abrasive, jagged edges of the dust on the lunar surface. The simulant has been developed to closely match the chemical composition and mineralogy of lunar dust. Table 1 shows the weight percent of the key minerals of interest in the LMS-1D simulant for their spectral properties discussed in Section 1.2. In addition, the $SiO_2$ chemical compound is highlighted for its characteristic Raman peak. $SiO_2$ has a chemical composition wt% of 51.2 [4].

*1.2 Spectral properties of lunar regolith*

Previous work has shown that spectral peaks of various ceramics respond to stress, damage, and temperature changes [5-10]. The calibration of $Cr^{3+}$ photo-luminescence of alumina with stress, for example, has been leveraged to develop nanocomposite sensors that can be used for stress and damage sensing [7,8]. The intensities from the spectral peaks have been used to quantify the dispersion of reinforcing ceramic particles in composites [9,10]. Spectral properties of lunar regolith have been reported sparsely in literature [5-8, 11-13] and are highlighted in Table 1. Since these peaks correspond to minerals that have been studied in their individual form, expected sensitivities of their Raman peaks for future investigation are provided. The potential for lunar regolith simulants to be tailored as sensors, in a similar way as ceramics, is the focus of investigation in this work.

Table 1. Expected Raman peaks of minerals/chemical compound constituents of interest and their weight percent in Lunar regolith (LMS-1D) [4-6,12-15]. Expected sensitivity for potential sensor development are listed. wt% is provided for mineralogy.

| Mineral/ Compound | wt% | Raman (cm$^{-1}$) | Expected Sensitivity |
|---|---|---|---|
| Pyroxene | 32.8 | 228,338,657, 679,995,1007 | Luminescence |
| Glass-rich Basalt | 32 | 757,970 | - |
| Anorthosite | 19.8 | 198,285,404, 504 | - |
| Olivine | 11.1 | 819,848 | Thermo-luminescence |
| Ilmenite | 4.3 | 681 | - |
| $SiO_2$ | - | 520 | Stress, Temperature |

*1.3 Considerations for In-space manufacturing*

When considering the lunar environment, the approach of using Raman and Luminescence spectroscopy as measurement methods is robust and well tested [11-13]. Therefore, the operation of functional sensors in space that depend on spectral response of lunar regolith to external stimuli, such as stress and temperature, are not anticipated to be affected by the lunar environment. However, in-space manufacturing of these functional sensors is of interest in order to avoid cost, volume, and up-mass constraints. When manufactured in low-gravity environments, for purposes of in-situ resource utilization, there will be differences in material and potentially sensor properties, when compared to manufacturing on Earth. These differences are likely to be dependent on the manufacturing process.

Samples studied in this work are based on two manufacturing approaches. Firstly, 3D printing of regolith-loaded resin, cured using Digital Light Processing (DLP), and secondly manufacturing of regolith using a binderless sintering process. In each of these processes, it is anticipated that the properties achieved in the investigations described here are likely to be affected in different ways when manufacturing in a low-gravity environment. However, prior to studying the effects of microgravity on the manufacturing processes, it is valuable to assess how each of these manufacturing processes influences the measured spectral emissions and mechanical properties of the sensor. This may enable the processing approach to be more clearly

defined prior to low-gravity studies that will be conducted in the future.

Additionally, building on the principles of elastic thermobarometry, the equations of state and elastic properties of regolith particles can be leveraged to convert measured strains into estimates of the pressure-temperature conditions experienced by the material [16]. This is possible due to the contrasting compressibility and thermal expansivities resulting from thermal cycling or applied loads, which induce differential strains between the matrix and its inclusions. These strains can be quantified in situ using Raman spectroscopy, effectively transforming regolith composites into functional sensors.

With these considerations in mind, we initiate the investigation, in this work, to develop functional sensors from lunar regolith. This is accomplished by exploring spectral properties of samples manufactured using two different approaches. The effect of the manufacturing processes on the spectral properties that are of significance for sensor creation is the focus of the results presented. The mechanical properties of these sensors are also of interest for their longevity under harsh lunar conditions. The ground reference study conducted in this work will provide an insight into differences in manufacturing of the regolith sensors and their spectral behavior, paving the way to future systematic assessments of the impact of low-gravity environment on manufacturing and consequent sensor performance using an optimized processing approach.

## 2. Material and methods

The materials, manufacturing processes, Raman measurement parameters and mechanical testing method are explained in the following sections. The LMS-1D simulant was manufactured into samples using two separate processing approaches described here and the samples for each were investigated using Raman spectroscopy. Mechanical testing was conducted to assess sensor material strength under compressive loads.

### *2.1 Lunar regolith resin printing with DLP*

In the first approach a resin-regolith (Zyltech-LMS-1D) composite was manufactured via Digital Light Processing (DLP) 3D printing. The desired regolith weight fraction selected was 10 wt% with the goal of enabling sufficient particle concentration for spectral data, while maintaining the structural integrity of the sample to avoid brittleness and delamination.

The optical image of the resin-regolith DLP sample is shown in Figure 1. The vertical line patterns observed with the partial ring Epi-illuminated microscope is a characteristic feature of DLP printing, as the curing process occurs layer by layer, leading to the visible texture in the final sample.

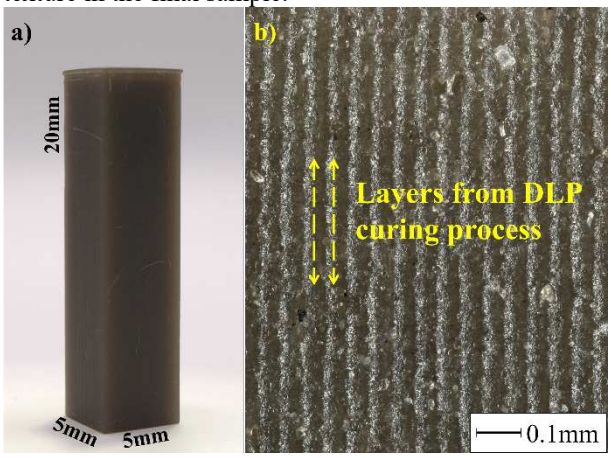


Fig. 1 DLP printed LMS-1D sample camera image (a) and optical micrograph of the surface (b) Vertical layers are features resulting from the DLP printing process.

In the mixing process, the desired amount of resin and regolith were added together and thoroughly mixed under a fume hood. The THINKY mixer AR-100 was used for the mixing process with three minutes of mixing, ensuring particle dispersion. Three minutes of defoaming helped to mitigate entrapped microbubbles within the matrix. After mixing, the suspensions were stored in dark containers to avoid light and airflow. Samples were then printed using a DLP printer with a 5 µm layer thickness and cured with 405 nm UV light for 6 seconds per layer. Post-processing included an isopropyl alcohol wash and additional UV curing for 3 minutes on each side of the sample. The parallelepiped samples of 10% wt fraction, with a square cross-section of 5mm and 4:1 aspect ratio, produced by this approach are referred to in the paper as the DLP samples.

### *2.2 Lunar regolith binderless sintering*

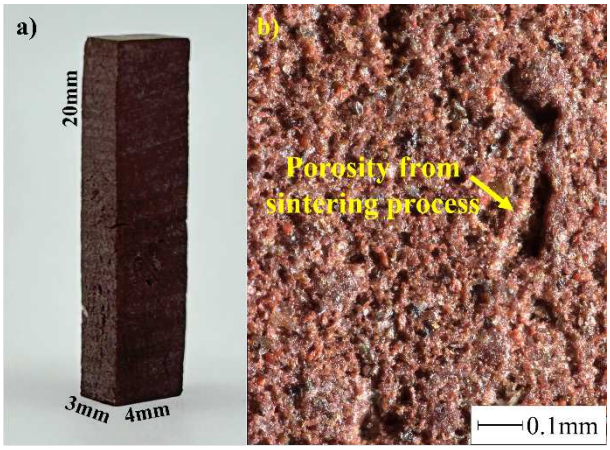


Fig. 2 Sintered LMS-1D sample camera image (a) and optical micrograph of the surface (b).

In the second approach, the LMS-1D was consolidated without a binder and sintered at 1150°C. The sintered samples were then machined using a diamond wire-cutter to produce parallelepiped parts of 3mm width, 4 mm height, and 20 mm length. The samples were polished and then investigated using optical microscopy and a representative image is shown in Figure 2. It is observed that although the sample was polished, some areas remained rough due to inherent porosity in the material.

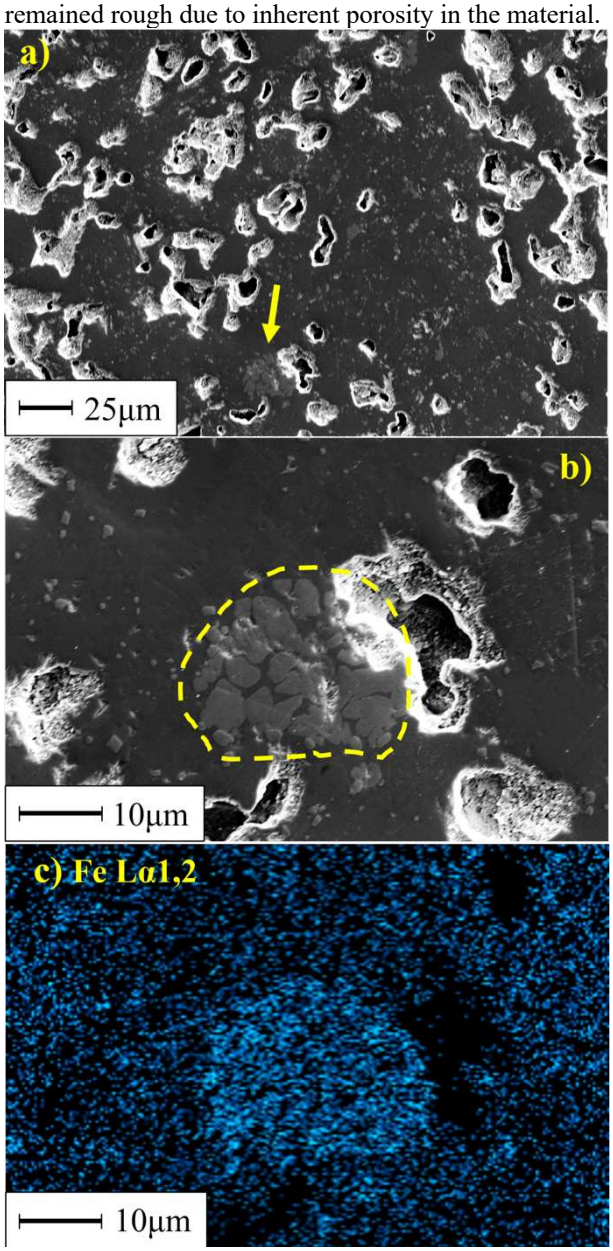


Fig. 3 SEM images of binderless sintered sample: (a) Overall surface morphology, bright areas indicate inherent porosity (b) High-magnification image of pores and surrounding microstructure, featuring a Fe-rich region indicated by dashed line, (c) EDS map of Fe

SEM images in Figure 3 show porosity more clearly on the sample's surface. The dense part between the pores indicates that general consolidation of particles has occurred during the sintering process, since no individual powder particles were discernible. The pores vary in size and shape with dimensions of about 5 to 20 µm. Some of the constituent elements segregate during the sintering process, resulting in regions with varying elemental composition, such as an iron-rich region observed in Figure 3c using EDS.

*2.3 Raman Spectroscopy measurements*

The Raman measurements were collected using a WITec Alpha 300RA Confocal Raman microscope equipped with a He:Ne 532 nm laser excitation source. The lens used for the measurements was a Zeiss EC Epiplan-Neofluar Dic 100x. The excitation laser power of 10 mW, 1800 g/mm grating and additional collection parameters, including 20 accumulations of 2 seconds integration time, remained constant throughout the measurements. The Raman data was then analyzed using a Python code for background subtraction and processing.

*2.4 Lunar regolith mechanical testing*

Compressive tests were performed on the parallelepiped specimens cut from sintered regolith material. The specimens had a nominal cross section of 3 mm x 4 mm and a length of 20 mm. An electro-mechanical universal testing machine (Instron LLC), equipped with a 10 kN load cell, was used for applying the load. The specimens were clamped between to plan parallel plates, and a compressive load was applied along the length axis of the specimens. The compressive tests were displacement controlled with a displacement rate of 5 mm/min. The displacement and the load were recorded and the stress-strain behavior was analyzed. Further, videos of the experiments were recorded. Future compressive tests will be conducted on the DLP samples which are estimated to be about one order of magnitude lower in strength than the sintered samples due to the low volume fraction of regolith.

## 3. Theory

Measurements of stress, damage and temperature can be achieved using optical measurements from luminescence or Raman emissions of ceramic materials. The corresponding theory related to these relationships is described in the following sections.

*3.1 Spectroscopy for stress and damage sensing*

The Raman peak of silicon at 520 $cm^{-1}$ is known for its shift with the application of stress. Similarly, the photo-luminescence lines in chromium-doped sapphire have been calibrated for their peak shift with applied stress. For the case where these ceramics are deployed as particles within a composite, the shift $\Delta\nu$ can be

measured against a strain gage measurement of the composite. The transformation between the two measurements can then be shown to be a combination of ratios in Equation (1) that can be analytically established based on the mechanical properties of the luminescent particle and the composite. This relationship is usually defined as the composite's piezospectroscopic coefficient ($\prod_c$). Calibration measurements can experimentally establish the coefficient [17].

$$\Delta\nu = \frac{\Delta\nu}{\varepsilon_{ii}^{p}}\frac{\varepsilon_{ii}^{p}}{\varepsilon_{ii}^{c}}\frac{\varepsilon_{ii}^{c}}{\varepsilon_{1}^{c}}\varepsilon_{1}^{c} = \Pi_c\varepsilon_{1}^{c} \quad (1)$$

Distribution of intensities collected from the composite can identify variation in the dispersion of particles in samples manufactured [9,10].

*3.2 Temperature sensing using thermoluminescence*

In phosphor thermometry, the temperature sensitivity of the luminescence of transition metals or rare-earth elements that are added as dopants in host materials is used to establish temperature [8]. Rare earth elements have been utilized for their luminescence decay with the objective of developing temperature-sensing capabilities [8]. The natural thermoluminescence (TL) of lunar regolith can be used in a similar way to measure temperature [13,14]. The excitation of the luminescent material by a laser source of a particular wavelength is selected based on the absorption spectra of the material. The decay in intensity is represented in Equation 2 [14].

$$I(T) = n_o s e^{\left(-\frac{E}{kT}\right)} e^{\left\{-\int s e^{\left(-\frac{E}{kT}\right)/\beta}\right\} dT} \quad (2)$$

$E$ (eV) is the activation energy for electrons to escape a trap in the crystal lattice, and $s$ ($s^{-1}$) is an Arrhenius factor for the probability of an electron escaping the trap.

## 4. Results and Discussion

The results of the Raman measurements and the mechanical tests are presented and discussed in the context of the different manufacturing approaches.

*4.1 Results of Raman spectral properties*

Figure 4 shows the Raman spectra of the samples from each manufacturing approach compared with raw powder along with a number of peaks marked. The minerals described in Table 1 are identified in the spectra of Figure 4.

As a first observation, the Raman peaks from the spectral data of raw powders are generally conserved in the parts manufactured using either one of the two processes. The spectral intensities are seen to vary differently in each of the DLP and sintered samples.

In the case of Anorthosite, which is primarily composed of Anorthite, a calcic plagioclase feldspar, a characteristic doublet around 504 $cm^{-1}$ is observed. While the intensity of this doublet decreases in both manufactured samples, it remains more distinct in the DLP-printed sample. The UV curing process in DLP printing may have induced residual stress on the particles due to the solidification of the surrounding matrix, contributing to the clear differentiation of the doublet. Similarly, residual stress could be introduced in the sintering process due to high consolidation temperatures, leading to broader and shifted peaks.

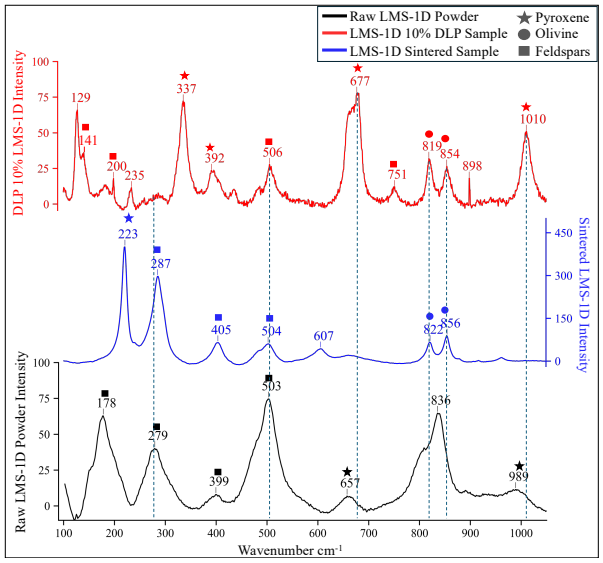


Figure 4: Raman peak wavenumber ($cm^{-1}$) and corresponding intensities (CCD counts) of LMS-1D samples, including raw powder (bottom black curve), sintered samples (middle blue curve), and DLP-printed 10% wt composite (top red curve). Known mineral peaks are indicated, with pyroxene (stars), olivine (circles), and feldspars (squares) marked for reference.

The linewidth of full width half maximum (FHWM) is wider for the raw powders, and the emergence of clear peaks for the DLP sample is due to the more distinct narrow wavelengths. The linewidth is typically representative of grain sizes but is also affected by residual stress.

The emergence of some of the peaks is likely due to the changes in peak positions and linewidths making some broad peaks appear. Peak shifts are seen for a number of the minerals such as Olivine. A further analysis may demonstrate the amount of peakshift for each of the identified peaks. Calibration of the intensity ratios, peak

positions and linewidth with temperature and stress is the next step for the development of sensing properties.

*4.2 Results of mechanical tests*

Fig 5 shows the stress-strain plots for the various samples. The achieved maximum stress for the batch of 7 samples showed a wide scatter with an average 67.4 MPa and a standard deviation of 25.3 MPa.

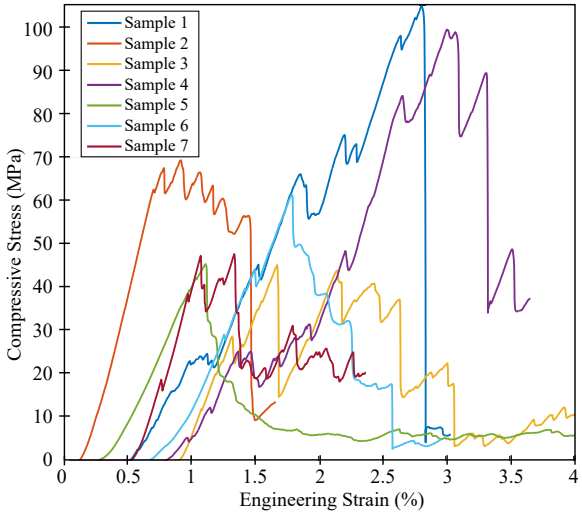


Figure 5: Stress-strain plots from the 7 samples of sintered regolith demonstrating the variation and load drops.

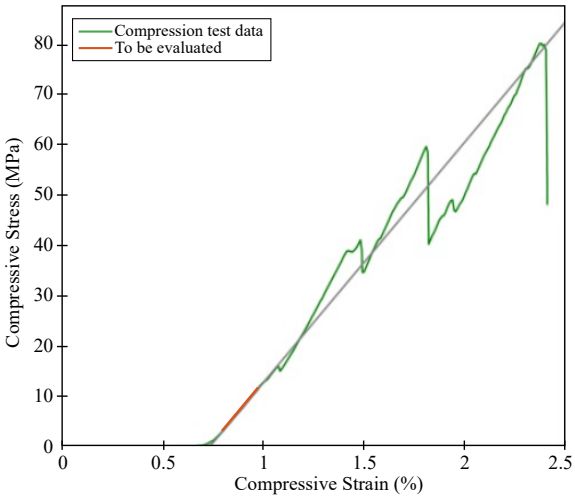


Figure 6: Exemplary stress-strain curve of compressive tests on sintered lunar regolith, showing load drops due to crack formation

An exemplary stress-strain curve of sintered regolith is displayed in Figure 6. During loading, repeated load drops occurred, and by means of the recorded videos, the load drops have been assigned to the formation of cracks. Chipping of small flakes and vertical cracking was observed. Figure 7 shows a video screenshot of a specimen with a longitudinal crack which occurred shortly before final failure.

For the mechanical tests, the observed scatter of compressive strength data can be attributed to deviations of the specimen geometry from an ideal rectangular block. The loaded faces of the specimens were not exactly plane parallel which resulted in inhomogeneous stress distribution at the contact to the loading plates, crack formation and chipping of material. Therefore, the observed failure stresses are below the compressive strength, specimens of the sintered regolith can achieve, if the specimen preparation will be improved.

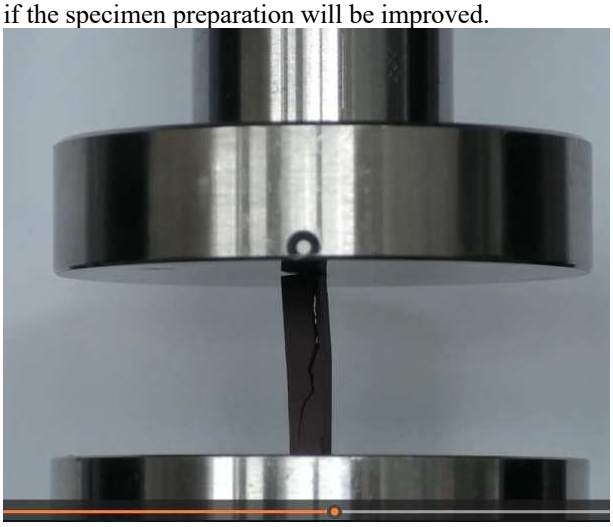

Figure 7: Video-screenshot of a specimen with a longitudinal crack which occurred shortly before final failure.

## 5. Conclusions

In conclusion, the viability of obtaining distinct spectral peaks was successfully demonstrated using regolith manufactured through two different approaches. The samples exhibited consistent, and in some cases enhanced, Raman shift signals for key mineral groups such as olivine, feldspars, and pyroxene. Differences in Raman peak characteristics between samples could be attributed to the different manufacturing parameters; for instance, the sintered samples reached temperatures as high as 1150°C, while the resin-based composites may have experienced mechanically induced shifts during the curing process. This demonstrates not only the feasibility of optimizing sensors for specific applications but also the potential for selectively manufacturing regolith materials with compositions that exhibit the desired sensitivity for tailored sensor functionality.

The mechanical testing demonstrated that the average compressive strength of the sintered regolith samples falls in the range of samples manufactured for construction. This is expected to significantly exceed that

of lunar resin-regolith DLP samples, which will be tested in future experiments.

Considering the manufacturing in space, it is anticipated that although all Raman measurements are unaffected by low gravity, there will be changes to the spectra. These will likely be caused by different effects of heating and flow during the sintering or curing process in a low-gravity environment. In general, there is strong potential for creating functional sensors from lunar regolith that can support operations in space. Future investigations to optimize the manufacturing process and calibrate the response of the spectra with external stimuli will be conducted.

**Acknowledgements**

This material is based upon work supported by National Science Foundation grants CMMI 2349931, OISE 1952523 and by the German Aerospace Center (DLR). The authors thank B. Fekadu and N. Seiler from DLR for their support in performing the mechanical tests

*Any opinion, findings, and conclusions or recommendations expressed in this material are those of the authors and do not necessarily reflect the views of the National Science Foundation.*

**References**

[1] Peter J. Collins, Jennifer Edmunson, Michael Fiske, Aleksandra Radlińska, “Materials characterization of various lunar regolith simulants for use in geopolymer lunar concrete,” Advances in Space Research,Volume 69, Issue 11, 2022, Pages 3941-3951, ISSN 0273-1177,

[2] Peter Warren, Nandhini Raju, Hossein Ebrahimi, Milos Krsmanovic, Seetha Raghavan, Jayanta Kapat, Ranajay Ghosh, “Effect of Sintering Temperature on Microstructure and Mechanical Properties of Molded Martian and Lunar Regolith” Ceramics International, 2022.

[3] Radl, A., Milicevic Neumann, K., Wotruba, H. et al. From lunar regolith to oxygen and structural materials: an integrated conceptual design. CEAS Space J 15, 585–595 (2023).

[4] A. Madison, Z. Landsman, J. Long-Fox, A. Metke, K. Krol, P. Easter, C.Sipe, L. Weber, D. Britt, “Lunar Dust Simulants and Their Applications”, Proceedings of Earth and Space 2022.

[5] P Latorre, S Raghavan, Q Fouliard “Manufacturing sensors using celestial body regolith”, US Patent App. 18/229,572, 2024

[6] Marc Fries and Andrew Steele “Raman spectroscopy and confocal Raman imaging in mineralogy and petrography” Inbook Confocal Raman Microscopy, Springer Series in Optical Sciences 158:111-135, January 2011,

[7] Amanda Stevenson, #Ashley Jones, and *Seetha Raghavan, “Stress-Sensing Nanomaterial Calibrated with Photostimulated Luminescence Emission”, Nano Letters, 11 (8), pp 3274– 3278, 2011.

[8] Quentin Fouliard, Johnathan Hernandez, Bauke Heeg, Ranajay Ghosh, Seetha Raghavan, “Phosphor Thermometry Instrumentation for Synchronized Acquisition of Luminescence Lifetime Decay and Intensity on Thermal Barrier Coatings” Measurement Science and Technology, 31(5), 054007,2020.

[9] Imad Hanhan, Alex Selimov, Declan Carolan, Ambrose Taylor, *Seetha Raghavan,“Quantifying Alumina Nanoparticle Dispersion in Hybrid Carbon Fiber Composites Using Photoluminescent Spectroscopy”, Applied Spectroscopy, January 1, 2016.

[10] Amanda Stevenson, Ashley Jones, *Seetha Raghavan “Characterization of Particle Dispersion and Volume Fraction in Alumina-Filled Epoxy Nanocomposites Using Photo-Stimulated Luminescence Spectroscopy” Polymer Journal, 43 (11), pp. 923-929, 2011. (Selected as feature article)

[11] S. Zhao, L. Xiao, Y. Qian, J. Zhao, Z. She, Q. He, Z. Wang, X.Wang, K. Cao, X. Zeng, Y. Wang, J. Sun, M. Dong, Q. Xiao, Z. Yin, H. Yang, J. Zhao, J. Wang, J. Huang, Z. Hu, K. Zong, X. Wu, C. Wang, “Variations in lunar regolith properties with depth as revealed by Chang'e-5 samples”, Icarus, Volume 406, 2023.

[12] Z.C. Ling, Alian Wang, Bradley L. Jolliff “Mineralogy and geochemistry of four lunar soils by laser-Raman study” Icarus 211,101–113 (2011).

[13] A. Sehlke, D. W. G. Sears, and the ANGSA Science Team. Lunar regolith thermoluminescence glow curve fitting to extract its most important kinetic parameters.54th Lunar and Planetary Science Conference 2023

[14] Durrani et al. LPSC VII. Proc. 1157, (1976).

[15] Freeman, J. et al., “Characterization of Natural Feldspars by Raman Spectroscopy for Future Planetary Exploration,” The Canadian Mineralogist, Vol. 46, 2008, pp. 1477–1500.

[16] Kohn, Matthew J.; Mazzucchelli, Mattia L.; and Alvaro, Matteo, ”Elastic Thermobarometry". Annual Review of Earth & Planetary Sciences, 51, 331-366. (2023)

[17] Gregory Freihofer, Axel Schülzgen, and Seetha Raghavan. Multiscale mechanics to determine nanocomposite elastic properties with piezospectroscopy. Acta Materialia, 81:211218, 2014.